Surface driven biomechanical breast image registration

Björn Eiben, Vasileios Vavourakis, John H. Hipwell, Sven Kabus, Cristian Lorenz, et al.

Björn Eiben, Vasileios Vavourakis, John H. Hipwell, Sven Kabus, Cristian Lorenz, Thomas Buelow, Norman R. Williams, M. Keshtgar, David J. Hawkes, "Surface driven biomechanical breast image registration," Proc. SPIE 9786, Medical Imaging 2016: Image-Guided Procedures, Robotic Interventions, and Modeling, 97860W (18 March 2016); doi: 10.1117/12.2216728

SPIE.

Event: SPIE Medical Imaging, 2016, San Diego, California, United States

Surface Driven Biomechanical Breast Image Registration

Björn Eiben[a], Vasileios Vavourakis[a], John H. Hipwell[a], Sven Kabus[b], Cristian Lorenz[b], Thomas Buelow[b], Norman R. Williams[c], M. Keshtgar[d], and David J. Hawkes[a]

[a] Centre for Medical Image Computing, UCL, Gower Street, London, WC1E 6BT, UK,
[b] Philips Research Laboratories, Röntgenstrasse 24-26, 22335 Hamburg, Germany,
[c] Surgical & Interventional Trials Unit, UCL, 132 Hampstead Road, London, NW1 2BX, UK,
[d] Department of Surgery, Royal Free Hospital, Pond Street, London, NW3 2QG, UK

ABSTRACT

Biomechanical modelling enables large deformation simulations of breast tissues under different loading conditions to be performed. Such simulations can be utilised to transform prone Magnetic Resonance (MR) images into a different patient position, such as upright or supine. We present a novel integration of biomechanical modelling with a surface registration algorithm which optimises the unknown material parameters of a biomechanical model and performs a subsequent regularised surface alignment. This allows deformations induced by effects other than gravity, such as those due to contact of the breast and MR coil, to be reversed. Correction displacements are applied to the biomechanical model enabling transformation of the original pre-surgical images to the corresponding target position.

The algorithm is evaluated for the prone-to-supine case using prone MR images and the skin outline of supine Computed Tomography (CT) scans for three patients. A mean target registration error (TRE) of 10.9 mm for internal structures is achieved. For the prone-to-upright scenario, an optical 3D surface scan of one patient is used as a registration target and the nipple distances after alignment between the transformed MRI and the surface are 10.1 mm and 6.3 mm respectively.

Keywords: breast cancer, biomechanical modelling, surface alignment, registration, large deformation simulation, finite elements

1. INTRODUCTION

Breast cancer is the most common cancer for women worldwide and in the UK women bear a lifetime risk of one-in-eight to develop this disease. Detection, diagnosis and interventions could benefit from combining information from different images or aligning images and the contained information with a surgical or interventional setting. To achieve this goal, establishing accurate correspondence between images or between images and a real world setting is required. The breast is a soft organ and is subject to large deformations when the patient position is changed. Different procedures require different patient setups to optimise image acquisition (e.g prone Magnetic Resonance Imaging), improve patient stability and comfort (e.g supine radiotherapy treatment) or account for practical circumstances (e.g. supine surgical position).

Prone-to-supine breast image registration aims to establish correspondence between images in the presence of large deformations. Standard intensity based image registration alone is unlikely to produce sufficient alignment due to the lack of initial overlap between the images. However since gravity is the main source of breast deformation between patient positions, solid mechanics can be exploited to predict gravity induced deformations. Such deformations can in turn be effectively used to guide registration procedures.[1] While some published approaches use mechanical simulations alone to predict one patient configuration from the other[2–4] alternative strategies combine biomechanical simulations with standard image registration methods[5–8] or aim for a higher level of integration between simulation and registration.[9]

Pre-surgical prone Dynamic Contrast Enhanced (DCE) MR images are part of the standard clinical procedure for some patients and provide important information about the extent and location of the cancerous tissue. This motivates the use of DCE MR images to guide surgical procedures. In the current clinical workflow however, 3D prone-supine image pairs are usually not available at the time of surgery, which potentially limits the use of

Medical Imaging 2016: Image-Guided Procedures, Robotic Interventions, and Modeling,
edited by Robert J. Webster III, Ziv R. Yaniv, Proc. of SPIE Vol. 9786, 97860W
 · doi: 10.1117/12.2216728

image driven registration approaches. Supine CT images for instance are only acquired after surgery to facilitate planning of dose delivery for radiotherapy. Another challenge related to the clinical applicability of patient-specific biomechanical models is that the material parameters are often not known and wide stiffness variations are reported in the literature. This motivated material parameter optimisation (see e.g. Han et al.[8]).

In the context of image guided breast surgery, supine breast MRI[10] might provide information about the extent and location of a lesion in the surgical position. Hence this configuration was utilised in studies to assess the feasibility of image guided breast interventions.[11,12] However, to date the supine imaging position is not standard clinical practice.

Optical surface imaging techniques have become popular in recent years. This fast, non-invasive and, compared to MRI, relatively low cost imaging modality could be used to image the patient in an upright or supine surgical pose. This could provide a valuable adjunct to prone pre-operative MRI, for surgical planning, surgical guidance or cosmetic evaluation when the prone image is warped to a target surface.

We propose an image-to-surface registration method which incorporates finite element (FE) biomechanical modelling, material parameter optimisation and surface warping to transform prone MR images to a supine or upright target surface. For validation purposes the target surface is extracted from a supine radiotherapy planning CT scan, to allow evaluation of the TRE within the breast volume. To evaluate the method with an upright 3D surface scan, alignment accuracy is measured using the nipple position.

2. MATERIAL AND METHODS

2.1 Image Data and Landmarks

Pre-surgical structural T1 and T2 weighted MR images with a native resolution of $0.7 \times 0.7 \times 3.0\,\mathrm{mm}^3$ were acquired in the context of the VPH-PICTURE project* and patient consent was obtained. For the same patients supine CT images with a resolution of $1.1 \times 1.1 \times 3.0\,\mathrm{mm}^3$ were acquired after breast conserving surgery as part of the radiotherapy planning procedure. In addition for case P1 an upright surface scan was obtained using a 3dMD optical acquisition system†.

In order to evaluate the alignment quality between prone and supine images, corresponding landmarks were manually selected in MR and CT images in the not operated breast, i.e. contralateral side, to avoid effects of tissue removal between the images. Since manual landmark selection is difficult, a control observer was given the prone landmarks of the first observer and asked to identify the corresponding locations in the supine position. Supine landmarks which were more then 15 mm apart were excluded from the evaluation to obtain more reliable landmarks.

2.2 Image Segmentation and Biomechanical Model

Prone MRI and supine CT images are segmented by first delineating the patient's skin surface. MR images are further processed and the surface of the pectoralis muscle is identified to define the posterior boundary of the biomechanical model. Internal breast structures are then further segmented into adipose and fibro-glandular tissues using *niftyseg*‡, an expectation maximisation based image segmentation. With the segmentation in place, the breast geometry is discretised into an FE mesh consisting of tetrahedral volume elements to represent the breast tissue and triangular membrane elements to represent the skin. Each element is labelled according to the tissue class segmentation result. The constitutive relation for the adipose and fibroglandular tissue was selected to be

$$\bar{W}_{\mathrm{tissue}} = \frac{\mu}{2}\left(\bar{I}_1 - 3\right) + \frac{\kappa}{2}\left(J-1\right)^2, \tag{1}$$

where μ and κ are the material parameters in terms of the shear and bulk modulus respectively, J is the determinant of the deformation gradient, and $\bar{I}_1$ is the first invariant of the deviatoric right Cauchy-Green tensor. The skin is modelled as a membrane, using the following exponential constitutive expression[13]

$$\bar{W}_{\mathrm{skin}} = \alpha_s\left(e^{\beta_s(\tilde{I}_1-3)} - 1\right) + c_s(\tilde{I}_2 - 3), \tag{2}$$

*http://www.vph-picture.eu

†http://www.3dmd.com

‡http://sourceforge.net/projects/niftyseg/

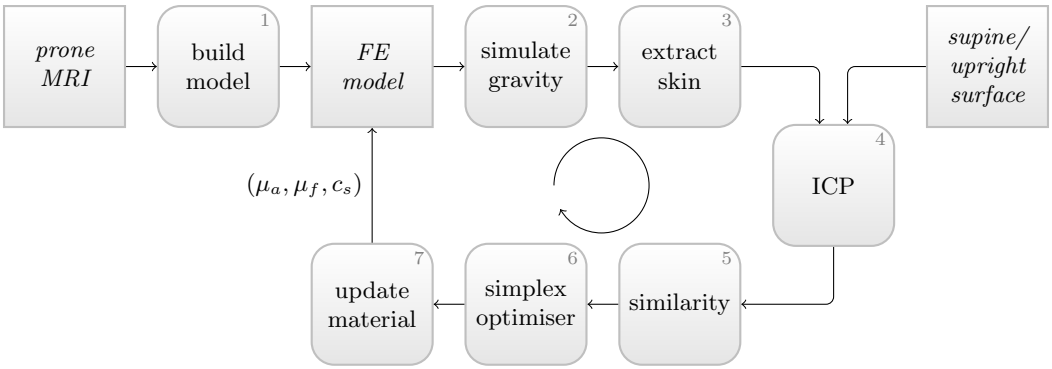

Figure 1. Overview of the material parameter optimisation workflow that aligns the finite element biomechanical model with the supine (or upright) surface scan. The material parameters of the biomechanical model are optimised such that rigid alignment of the surface scan and the simulated corresponding position improves the similarity measure.

where $\tilde{I}_1$ and $\tilde{I}_2$ denote the first and second invariant of the two-dimensional Cauchy-Green strain tensor and α_s, β_s and c_s are material parameters. The boundary conditions of the breast model are selected such that the breast-chest interface is regarded as fixed, whereas the skin is assumed to be traction free. Nodes on the superior and inferior planes are restricted to axial in-plane motion. For the modelling purposes of this study, the open-source finite element solver *FEB3*[§] is utilised.

2.3 Material Parameter Optimisation

Figure 1 shows an overview of the material optimisation strategy which forms the first step of the proposed alignment procedure. The numbers given in the boxes are also used in the text at corresponding locations. The prone MRI based biomechanical model is generated (1) as described in section 2.2 and together with the target image forms the input to the optimisation.

The purpose of the optimisation procedure is to align the biomechanical model and the target surface as well as possible by only varying the material parameters of the biomechanical model. To this end a single multiplicative adipose/fibroglandular shear modulus factor is optimised, whilst maintaining a fixed ratio between the two tissue classes of $\mu_f = 1.5\mu_a$.[14] The bulk modulus κ on the other hand is set so that it resembles a constant Poisson's ratio of $\nu = 0.475$, which was found to be a good compromise between near incompressible tissue behaviour and simulation stability. For the skin we select c_s as the free parameter in the optimisation procedure since it is associated with $\tilde{I}_2$ which in turn can be interpreted as a measure for surface area change.

The biomechanical simulation (2) consists of two steps. In the first step the effect of gravity is removed by estimating an unloaded configuration.[15] In the second step gravity is re-applied corresponding to the configuration of the target surface (i.e. supine or upright). In the simulated target configuration the skin surface is extracted from the model (3) in order to facilitate rigid alignment with the target surface using an iterative closest point algorithm (ICP)[16](4). Since changes of the material parameters also affect the rigid alignment between the simulation and the target surface, the ICP is run repeatedly after each simulation.

The registration quality between the loading simulation and the target surface is evaluated with an objective function (5). For this purpose the mean Euclidean point-to-surface distance is used. Let $\mathbf{P}_{\text{sim}}(\mu_{\text{f}}, \mu_{\text{g}}, c_s) = \{\mathbf{P}_1, \mathbf{P}_2, \ldots, \mathbf{P}_N\}$ be the N points of the moving surface mesh, i.e. the extracted skin points of the biomechanical loading simulation. Furthermore let S_{scan} be the target surface, then the objective function is given by the mean minimum distance d of each point to the surface

$$m = \frac{1}{N} \sum_{i=1}^{N} d(\mathbf{P}_i, S_{\text{scan}}). \tag{3}$$

The outputs of the material optimisation workflow are the material parameters, as well as the homogeneous rigid matrix which is used to produce a transformed surface mesh S'_{rigid}.

[§]https://bitbucket.org/vasvav/feb3-finite-element-bioengineering-in-3d

The evaluation of the objective function (5) is computationally expensive as it includes two biomechanical simulations, and an iterative closest point registration (see figure 1). As a result the gradient of the objective function is not readily available. We use the gradient-free Nelder-Mead[17] simplex optimiser (6) to determine the updated material parameters (7).

2.4 Surface Warping

Optimised material parameters alone do not guarantee good alignment between the loading simulation and the corresponding scanned surface. This is due to the MRI scanning and patient support equipment. Even breasts of carefully positioned patients can show severe skin surface indentations especially in the medial region around the sternum.[18] To consider this deformation in the biomechanical unloading simulation, traction forces on the skin have to be defined. However, the local varying magnitude and direction of such forces is not known and thus cannot be introduced in the simulation. A simpler alternative is required. The residual alignment error of the loading simulation is corrected by imposing a displacement constraint on the skin nodes such that these nodes coincide with the skin target surface. A simple closest distance projection onto the 3D target skin surface however is insufficient since (i) the projection could result in significant surface area changes and in extreme cases in collapsing elements, (ii) the resulting surface elements could be of bad quality, and (iii) the displacements are not necessarily smooth. We have addressed each of the issues as follows.

The components of the proposed surface warping technique comprise a displacement calculation D, which drives the skin surface of the biomechanical model towards the target mesh, a Laplacian mesh smoothing step, L, which regularises the mesh, an area constraint, A, which reduces local changes in surface area and finally a self-intersection prevention, I, which avoids mesh intersections.

D: Displacement Let $\mathbf{K}$ be the nodal connectivity matrix of the skin surface mesh, then a matrix with smoothing characteristics can be computed by calculating its m_D-th power. Furthermore let the vector with the closest distances pointing from the current nodal positions $\mathbf{P}_i^{A,n}$ at iteration n to the surface S'_{scan} be $\mathbf{d} = \{\mathbf{d}_1(\mathbf{P}_1^{A,n}, S'_{\text{scan}}), \mathbf{d}_2(\mathbf{P}_2^{A,n}, S'_{\text{scan}}), \ldots\}$, then a smooth version of the displacements can be calculated according to $\mathbf{d}' = \mathbf{K}^{m_D}\mathbf{d}$. These smoothly varying displacements are used to update the nodal positions according to the following iterative scheme:

$$\mathbf{P}_i^{D,n} = \mathbf{P}_i^{A,n-1} + s\mathbf{d}'_i. \tag{4}$$

Here s is a scaling parameter which is used to balance the displacement driven component of the deformation with the other constraints.

L: Laplacian Mesh Smoothing Mesh regularity often is a desired quality in biomechanical simulations. To control this during the course of the iterations, *Laplacian Mesh Smoothing* is used (see e.g. the work by Field et al.[19] and references therein). This is particularly useful in cases where the simulated surface normal shows a large angle to the target surface. In such extreme cases the displacement step D could cause the moving elements to collapse. Hence let $w(\mathbf{P}_i^{D,n})$ be the set of indices of mesh points connected to point $\mathbf{P}_i^{D,n}$ and $|w|$ be the number of neighbours, then the displaced node $\mathbf{P}_i^L$ can be computed as

$$\mathbf{P}_i^{L,n} = (1-l)\,\mathbf{P}_i^{D,n} + \frac{l}{|w|}\sum_{j\in w}\mathbf{P}_j^{D,n}. \tag{5}$$

This means, that each point aims to move towards the centre of the surrounding points. The scalar weight l which in all processed cases was selected to be $l = 0.1$ controls the amount of smoothing.

A: Area Constraint Both previous mesh warping steps can introduce local changes to the surface area. In order to reduce the area change, a correction vector is calculated for each node as follows. Let $T = \{T_1, \ldots, T_j\}$ be the triangular surface elements connected to the current node $\mathbf{P}_i^{L,n}$. For each element a deviation from the

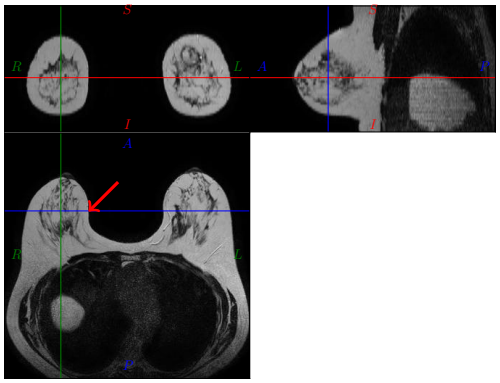

(a) Prone MR image

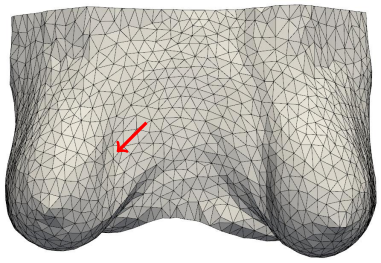

(b) Model surface after material optimisation

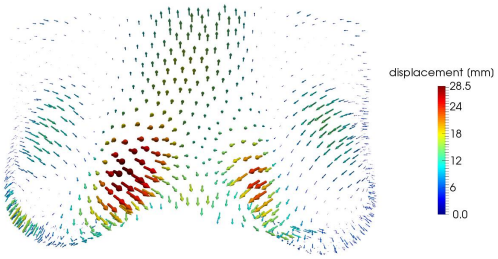

(c) Deformation vectors

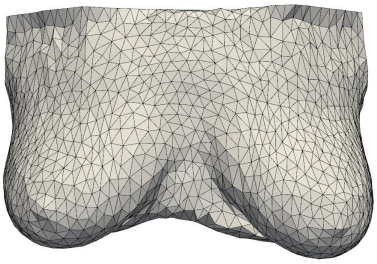

(d) Surface warping result

Figure 2. MRI and surface contact. (a) shows the prone MRI and the red arrow indicates contact of the breast with the coil. (b) is the simulated upright surface after the material optimisation step (c.f. section 2.3). The contact of the MRI breast coil propagates to the simulation result. To correct for this effect, a displacement vector field is calculated (c) as described in section 2.4. Application of the displacements to the simulated surface results in a corrected surface (d).

original surface area A_{0,T_m} (i.e. the area of each triangle before the surface warping is initiated) can be calculated

$$a_{T_m} = \frac{\|\mathbf{v}_{T_m} \times \mathbf{w}_{T_m}\|}{2A_{0,T_m}} - 1. \tag{6}$$

Here the vectors $\mathbf{v}_{T_m}$ and $\mathbf{w}_{T_m}$ point from the current central node to the opposite nodes of the triangle T_m. The final correction vector is calculated as

$$\mathbf{P}_i^{A,n} = \mathbf{P}_i^{L,n} + \sum_{t \in T} a_t \frac{\mathbf{v}_t + \mathbf{w}_t}{\|\mathbf{v}_t + \mathbf{w}_t\|}. \tag{7}$$

I: Intersection Prevention Updating the node positions can result in a self-intersecting mesh. This is most likely the case in the inframammary fold region when the upright position is used as a target configuration. Hence an intersection prevention process is incorporated by sensing possible surface contact in the direction of motion. If a self-intersection is detected, the corresponding node is kept fixed.

Figure 2 shows the impact of contact between the breast and the MR coil in the prone configuration and an example result of the surface warping methodology as described in this section. Note how the deformations that originate from contact of the patients' breast with the MRI coil are effectively reduced. The displacement vector field shows the largest amplitude in the medial breast region. Hence, the corrected mesh represents the actual upright surface more precisely (c.f. figure 4).

2.5 Volume Mesh Warping

In a final step the surface displacements calculated in section 2.4 are used to update the volume mesh of the biomechanical model with the optimised material parameters obtained in section 2.3. While a similar idea was

Table 1. Inter-observer landmark distance (IOD). All distance values are given in mm. The total number of landmarks and the number for which both observers were within 15mm of each other, are in given in the columns N_{all} and N_{15}.

	IOD all				IOD $d < 15$ mm			
Dataset	mean	max	std	N_{all}	mean	max	std	N_{15}
P1	16.7	41.4	12.8	15	8.2	14.0	5.0	9
P2	16.5	37.3	11.2	15	7.9	14.8	4.8	8
P3	12.8	52.2	12.8	12	7.5	14.1	3.6	10
P1-P3	**15.3**				**7.9**			

proposed by Ferrant et al.[20] with an application in brain-shift deformation recovery, here gravity loading and nodal displacement conditions are considered simultaneously. To calculate the volumetric displacements, the last loading simulation from the material parameter optimisation is re-initiated (c.f. step (2) in figure 1). When the gravity loading is completed, the displacement boundary condition on the skin surface nodes is activated. This imposes the previously calculated surface displacements onto the biomechanical simulation.

The volumetric displacements are now completely defined and can be generated by composing the deformation vector fields of (i) the unloading, (ii) the reloading, and (iii) the prescribed displacement simulations. This allows image warping and landmark transformation from the prone into the loaded configuration to be performed.

3. RESULTS

The evaluation of the registration method between prone MRI and supine CT surface was carried out using manually selected landmarks as described in section 2.1. The inter-observer distance (IOD) between the first and the control observer was evaluated for each prone MRI landmark by measuring the distance between the two observers' choice of corresponding supine CT landmark. Table 1 shows the results of the IOD evaluation. When all landmarks are considered, the mean IOD is between 12.8 mm and 16.7 mm. This value reduces to a range between 7.5 mm and 8.2 mm when only more reliable landmarks are considered for which both observers agree to a tolerance of 15mm.

Table 2 shows the TRE evaluated by using the sets of landmarks as described above. The TRE was measured between (i) rigidly aligned prone and supine datasets, (ii) the initial registration result, when generic material parameters were used, (iii) the TRE after material parameter optimisation, and (iv) the final result after surface warping. The overall mean TRE for IOD ($d < 15$ mm) using a rigid transformation only is 74.6 mm which is reduced by the supine simulation to 21.5 mm. The material parameter optimisation further reduces the TRE to 17.0 mm and the best overall accuracy of 10.9 mm is achieved after the surface warping step. When all landmarks are used to evaluate the alignment accuracy, the TRE measures 13.7 mm

Figure 3 shows the surface driven registration result for all cases investigated in this study. The skin surface was extracted from the supine CT surfaces (c.f. figures 3(a), 3(c), and 3(e)) and then used as the registration target for the prone MR images. The transformed MR images are shown in figures 3(b), 3(d), and 3(f). Note how structures in the healthy breast can be easily identified between corresponding images. For all cases the right breast is the healthy, not operated breast, shown on the left side of the figure.

The proposed method was also applied to register the MR image of P1 with the corresponding surface which was acquired with the patient standing in the upright position. Since the common features identifiable in the surface mesh and the MRI are limited to the nipples, the evaluation was carried out on this landmark only. Figure 4 shows the registration result as a volume rendering of the MRI combined with the textured 3D surface mesh (figures 4(a) and 4(b)). Figure 4(c) visualises the nipple locations identified in the transformed MRI as green spheres, whereas the nipple location on the skin surface is identified by cross hairs projected onto the skin surface. The measured Euclidean distances for the left and right nipples are 10.1 mm and 6.3 mm respectively.

4. CONCLUSIONS

Surface driven prone-to-supine registration with a future application in image guided surgery addresses the challenge that the target intra-operative data is not a three dimensionally resolved image, but an optical surface

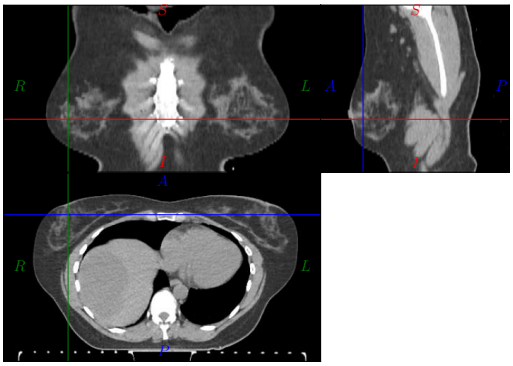

(a) P1: CT target

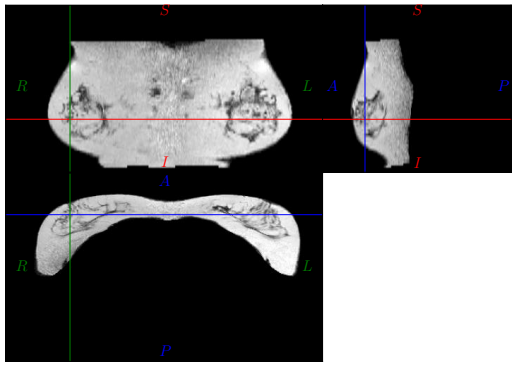

(b) P1: MRI image warped to supine.

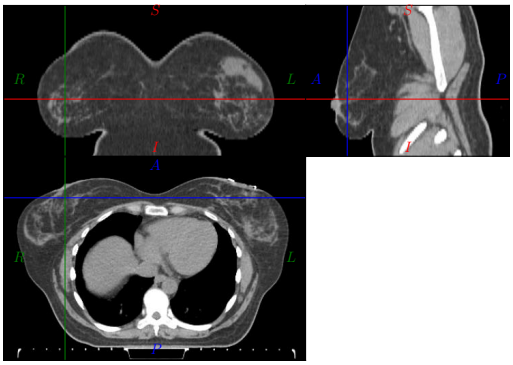

(c) P1: CT target

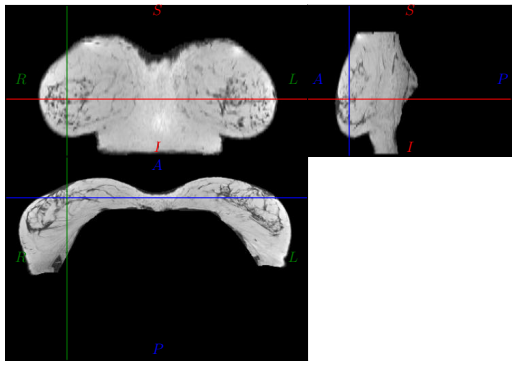

(d) P1: MRI image warped to supine.

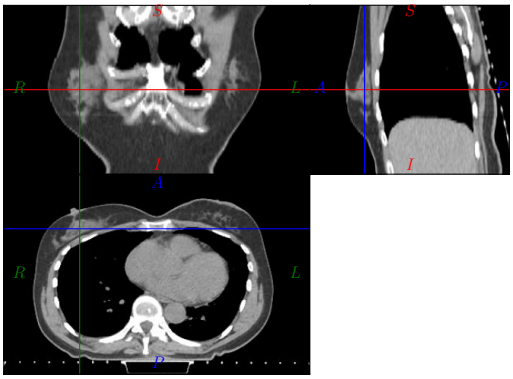

(e) P3: CT target

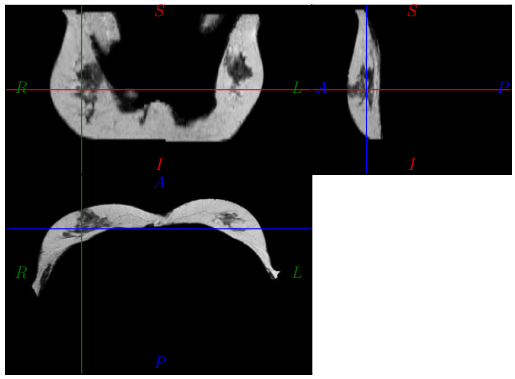

(f) P3: MRI image warped to supine.

Figure 3. Pure surface driven registration result. Common structures in the fiborglandular tissue can be easily seen in both, the target CT and the transformed MR image. Breast conserving surgery was carried out on the left breast (right side of the images above) which causes morphological changes to the breast tissue between the MRI and the CT acquisition. As a result evaluation of the registration performance was limited to the contralateral breast, indicated by the position of the cross hairs.

Table 2. TRE for (i) rigidly aligned prone and supine datasets, (ii) the registration result, when generic material parameters are used for the prone-to-supine registration, (iii) the TRE after material parameter optimisation, and (iv) the final result after surface warping. For each TRE measurement the mean, maximum and standard deviation is given in mm. The columns labelled *TRE all* report results for all landmarks from both observers, whereas columns labelled $d < 15$ mm exclude inconsistent landmarks, where the observers identified points further than 15 mm apart.

	(i) rigid (no simulation)							
	TRE all				TRE IOD $d < 15$ mm			
Dataset	mean	max.	std.	N_{all}	mean	max.	std.	N_{15}
P1	75.3	100.6	24.2	30	88.0	99.9	7.9	18
P2	106.6	131.8	19.0	30	101.6	125.5	18.0	16
P3	34.5	52.4	11.2	24	34.2	52.4	11.1	20
P1-P3	72.1				74.6			
	(ii) generic parameters							
	TRE all				TRE IOD $d < 15$ mm			
Dataset	mean	max.	std.	N_{all}	mean	max.	std.	N_{15}
P1	22.7	39.1	6.2	30	23.2	30.3	3.7	18
P2	31.7	67.5	11.8	30	27.0	35.4	5.5	16
P3	15.9	32.6	6.7	24	14.3	24.9	5.0	20
P1-P3	23.4				21.5			
	(iii) optimised parameters							
	TRE all				TRE IOD $d < 15$ mm			
Dataset	mean	max.	std.	N_{all}	mean	max.	std.	N_{15}
P1	19.6	33.4	5.5	30	19.0	26.0	4.0	18
P2	23.6	53.8	8.9	30	19.8	25.4	4.6	16
P3	14.0	34.0	6.9	24	12.2	21.4	4.5	20
P1-P3	19.1				17.0			
	(iv) optimised parameters and surface warping							
	TRE all				TRE IOD $d < 15$ mm			
Dataset	mean	max.	std.	N_{all}	mean	max.	std.	N_{15}
P1	12.1	35.4	8.4	30	9.1	18.7	4.8	18
P2	15.5	44.7	8.5	30	11.3	17.2	4.1	16
P3	13.6	28.6	7.1	24	12.3	24.0	5.7	20
P1-P3	13.7				10.9			

scan. Hence algorithms are required which enable the transformation of prone MR images into the supine position using target surface information.

We propose an integrated, biomechanically informed surface-driven registration methodology that overcomes two main challenges when biomechanical models are used to simulate the large deformation from prone to supine: (i) unknown material parameters and (ii) additional deformations introduced by the MRI scanning equipment in the prone position. This is achieved by a material optimisation procedure followed by surface warping step which corrects residual geometric differences between the biomechanical simulation and the target surface.

The alignment quality was measured in terms of the TRE by using manually selected internal breast landmarks. For the alignment between the prone MRI and the supine CT surface an overall mean TRE of internal structures was evaluated as 10.9 mm, despite no internal breast information being used to drive the registration. For a prone-to-upright application scenario the nipple distances between the transformed MRI and the surface scan measured 10.1 mm and 6.3 mm respectively.

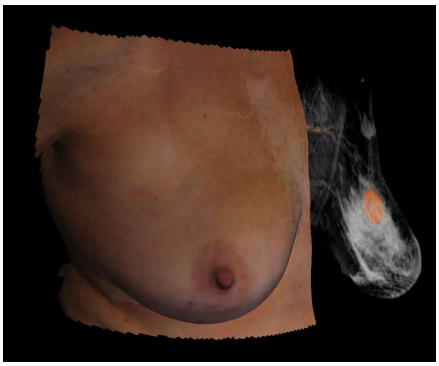

(a) Transformed MRI and target surface

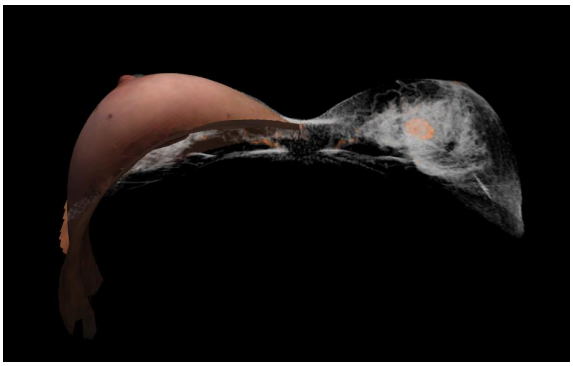

(b) MRI and target surface

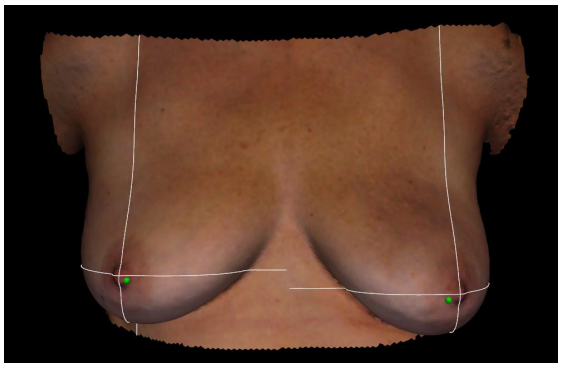

(c) Nipple locations

Figure 4. Surface driven registration result for a prone MRI to an upright optical 3D surface scan of the same patient. A volume rendering of the transformed MRI aligned with the surface is shown in (a) and (b), the tumour location clearly visible through appropriate choice of the transfer-function. Figure (c) shows the nipple locations identified in the warped MRI as green spheres and those in the surface scan as cross hairs.

The benefits of the surface driven approach are twofold. Regarding clinical application, the prone-supine registration can be utilised for surgical planning and initial guidance, since the lesion extent and margin visualisation becomes possible in multiple poses; namely supine, prone and upright. From the biomechanical modelling perspective the information obtained from the material optimisation and surface warping could be utilised in a feedback step to improve the biomechanical model geometry, by removing the MRI coil deformation artefacts. This in turn should lead to an updated and hence improved estimation of the unloaded configuration, increasing the fidelity and accuracy of subsequent biomechanical simulations.

Acknowledgment

We would like to thank Dominic Baxter, David Bishop, Emily Appleby, Immy Ashby, and Susan Smart from the Royal Free Hospital, London, for their tireless support during the PICUTRE study. This work is supported by funding from the European Community's Virtual Physiological Human Seventh Framework Programme under grant agreement: "PICTURE" (FP7-ICT-2011-9, 600948) and "VPH-PRISM" (FP7-ICT-2011-9, 601040); from the EPSRC grant "MIMIC": EP/K020439/1; and Philips Research Laboratories Hamburg. V. Vavourakis gratefully acknowledges the financial support of the Marie-Curie Fellowship "iBeSuP" (FP7-PEOPLE-2013-IEF, 627025).

REFERENCES

[1] Hipwell, J. H., Vavourakis, V., Han, L., Mertzanidou, T., Eiben, B., and Hawkes, D. J., "A review of biomechanically informed breast image registration," *Physics in Medicine and Biology* **61**(2), R1 (2016).

[2] Pathmanathan, P., Gavaghan, D. J., Whiteley, J. P., Chapman, S. J., and Brady, J. M., "Predicting tumor location by modeling the deformation of the breast," *IEEE Transactions on Biomedical Engineering* **55**(10), 2471–2480 (2008).

[3] Rajagopal, V., Nash, M., Highnam, R., and Nielsen, P., "The breast biomechanics reference state for multi-modal image analysis," in [*Digital Mammography*], Krupinski, E., ed., *Lecture Notes in Computer Science* **5116**, 385–392, Springer Berlin / Heidelberg (2008).

[4] Babarenda Gamage, T. P., Rajagopal, V., Nielsen, P. M. F., and Nash, M. P., "Patient-specific modeling of breast biomechanics with applications to breast cancer detection and treatment," in [*Patient-Specific Modeling in Tomorrow's Medicine*], Gefen, A., ed., *Studies in Mechanobiology, Tissue Engineering and Biomaterials* **09**, 379–412, Springer Berlin Heidelberg (2012).

[5] Lee, A., Schnabel, J., Rajagopal, V., Nielsen, P., and Nash, M., "Breast image registration by combining finite elements and free-form deformations," in [*Digital Mammography*], Martí, J., Oliver, A., Freixenet, J., and Martí, R., eds., *Lecture Notes in Computer Science* **6136**, 736–743, Springer Berlin / Heidelberg (2010).

[6] Carter, T., Tanner, C., Crum, W., Beechey-Newman, N., and Hawkes, D., "A framework for image-guided breast surgery," in [*Medical Imaging and Augmented Reality*], Yang, G.-Z., Jiang, T., Shen, D., Gu, L., and Yang, J., eds., *Lecture Notes in Computer Science* **4091**, 203–210, Springer Berlin / Heidelberg (2006).

[7] Eiben, B., Han, L., Hipwell, J. H., Mertzanidou, T., Kabus, S., Buelow, T., Lorenz, C., Newstead, G. M., Abe, H., Keshtgar, M., Ourselin, S., and Hawkes, D. J., "Biomechanically guided prone-to-supine image registration of breast MRI using an estimated reference state," in [*IEEE 10th International Symposium on Biomedical Imaging (ISBI)*], 214–217 (2013).

[8] Han, L., Hipwell, J. H., Eiben, B., Barratt, D., Modat, M., Ourselin, S., and Hawkes, D. J., "A nonlinear biomechanical model based registration method for aligning prone and supine MR breast images," *IEEE Transactions on Medical Imaging* **33**(3), 682–694 (2014).

[9] Eiben, B., Vavourakis, V., Hipwell, J. H., Kabus, S., Buelow, T., Lorenz, C., Mertzanidou, T., Reis, S., Williams, N. R., Keshtgar, M., and Hawkes, D. J., "Symmetric biomechanically guided prone-to-supine breast image registration," *Annals of Biomedical Engineering* **44**(1), 154–173 (2015).

[10] Siegler, P., Holloway, C. M., Causer, P., Thevathasan, G., and Plewes, D. B., "Supine breast MRI," *Journal of Magnetic Resonance Imaging* **34**(5), 1212–1217 (2011).

[11] Alderliesten, T., Loo, C., Paape, A., Muller, S., Rutgers, E., Peeters, M.-J. V., and Gilhuijs, K., "On the feasibility of MRI-guided navigation to demarcate breast cancer for breast-conserving surgery," *Medical Physics* **37**(6), 2617–2626 (2010).

[12] Conley, R. H., Meszoely, I. M., Weis, J. A., Pheiffer, T. S., Arlinghaus, L. R., Yankeelov, T. E., and Miga, M. I., "Realization of a biomechanical model-assisted image guidance system for breast cancer surgery using supine MRI," *International Journal of Computer Assisted Radiology and Surgery* , 1–12 (2015).

[13] Veronda, D. R. and Westmann, R. A., "Mechanical characterization of skin – finite deformations," *Journal of Biomechanics* **3**(1), 111–124 (1970).

[14] Tanner, C., Schnabel, J. A., Hill, D. L. G., Hawkes, D. J., Leach, M. O., and Hose, D. R., "Factors influencing the accuracy of biomechanical breast models," *Medical Physics* **33**(6), 1758–1769 (2006).

[15] Vavourakis, V., Hipwell, J. H., and Hawkes, D. J., "An inverse finite element u/p-formulation to predict the unloaded state of in vivo biological soft tissues," *Annals of Biomedical Engineering* **44**, 187–201 (2015).

[16] Besl, P. and McKay, N., "A method for registration of 3-D shapes," *IEEE Transactions on Pattern Analysis and Machine Intelligence* **14**(2), 239–256 (1992).

[17] Nelder, J. A. and Mead, R., "A simplex method for function minimization," *The Computer Journal* **7**(4), 308–313 (1965).

[18] Yeh, E. D., Georgian-Smith, D., Raza, S., Bussolari, L., Pawlisz-Hoff, J., and Birdwell, R. L., "Positioning in breast MR imaging to optimize image quality," *RadioGraphics* **34**(1), E1–E17 (2014).

[19] Field, D. A., "Laplacian smoothing and delaunay triangulations," *Communications in Applied Numerical Methods* **4**(6), 709–712 (1988).

[20] Ferrant, M., Nabavi, A., Macq, B., Jolesz, F. A., Kikinis, R., and Warfield, S. K., "Registration of 3-d intraoperative MR images of the brain using a finite-element biomechanical model," *Medical Imaging, IEEE Transactions on* **20**(12), 1384–1397 (2001).